Proceedings of ASME Turbo Expo 2016: Turbine Technical Conference and Exposition
GT2016
June 13–17, 2016, Seoul, South Korea

GT2016-57236

OPTIMIZATION OF ROBUST TRANSONIC COMPRESSOR BLADES

Marcus Lejon*
Division of Fluid Dynamics
Department of Applied Mechanics
Chalmers University of Technology
Gothenburg, Sweden
Email: marcus.lejon@chalmers.se

Niklas Andersson
Tomas Grönstedt
Division of Fluid Dynamics
Department of Applied Mechanics
Chalmers University of Technology
Gothenburg, Sweden

Lars Ellbrant
Hans Mårtensson
Division of Aerodynamics
GKN Aerospace Engine Systems
Trollhättan, Sweden

ABSTRACT

Surface degradation in an axial compressor during its lifetime can have a considerable adverse effect on its performance. The present study investigates how the optimized design of compressor blades in a single compressor stage is affected by considering a high level of surface roughness on a level representative of a long period of in-service use. It is shown that including surface roughness in the optimization process is of relatively little importance, however, matching of compressor stages is shown to require consideration as the rotational speed must be increased to reach the design point as surface quality decrease. An increased surface roughness in itself is shown to have a large effect on performance.

Two optimization approaches are compared. The first approach considers the compressor blades to be hydraulically smooth. The designs obtained from this approach are subsequently degraded by increasing the level of surface roughness. The compressor blades from the first approach are compared to designs obtained from a second optimization approach, which considers a high level of surface roughness from the outset.

The degraded compressor stages from the first approach are shown to be among the best performing designs in terms of polytropic efficiency and stability when compared to designs obtained with the second approach.

NOMENCLATURE

C_s	Roughness constant
$C_{p,rs}$	Static pressure recovery coefficient
κ	Von Karman's constant
k_s	Sand-grain roughness
k_s^+	Equivalent sand-grain roughness Reynolds number
M	Mach number
$\overline{P}$	Average pressure
p	Local static pressure
p_0	Total pressure
R	Radius
Re	Reynolds number
R_a	Arithmetic average surface roughness
S	Stability
u^+	Dimensionless velocity
u_τ	Wall friction velocity
υ	Kinematic viscosity
X	Axial coordinate
y^+	Dimensionless wall distance

Abbreviations

CFD	Computational Fluid Dynamics
Rel	Relative
RMS	Root Mean Square
dp	Design point
opt	Optimization
ps	Part speed
rpm	Revolutions per minute

*Address all correspondence to this author.

INTRODUCTION

An increase in surface roughness on axial compressor blades is known to reduce the performance and, consequently, increase the fuel consumption of a turbomachine. In the design phase, the surface of a compressor blade is typically assumed to be hydraulically smooth. However, once the aircraft engine is in service, surface degradation ensues as the engine is exposed to a wide range of environmental conditions where particles of varying sizes and compositions enter the air intake.

Sand grains were applied to the inside of pipes in [1] to study the effect of surface roughness on the wall boundary layer. The results are still in use today, and a measured level of surface roughness is often converted to an equivalent sand-grain roughness height when the effect of surface roughness is modeled in CFD.

The effect of surface roughness on the performance of NASA Rotor 37 was studied experimentally and numerically in [2] at subsonic and transonic conditions. The measured surface roughness was specified as 2.54 – 3.18 μm RMS. Different coatings were used to isolate the effect of surface roughness from the effect of the additional thickness of the coating on the blade geometry. While the stall line was shown to be unaffected by the coatings, the mass flow, total pressure ratio, and adiabatic efficiency were reduced. Compared to the baseline stage at 100% of design speed along a throttle line, a reduction in adiabatic efficiency of approximately 2.5 points could be attributed to the increase in surface roughness.

The effect of Reynolds number, surface roughness location and magnitude was experimentally investigated on a compressor cascade in [3]. The arithmetic average surface roughness R_a investigated in the study was specified to be in the range 0.38 – 2.89 μm. It was shown that an increase in surface roughness on the suction side had a more adverse effect on performance than an increase on the pressure side. It was also shown that loss increased rapidly when the Reynolds number exceeded 600 000 for the largest level of surface roughness investigated in the study.

Typical values of the center-line average of the surface roughness of the stator blades in a modern turbo-fan engine after a long period of in-service use are reported in [4] to be in the range 1.53 – 2.03 μm. It was shown that surface roughness has an adverse impact on performance, with a local increase in surface roughness near the leading edge and peak suction region having the largest impact. The surface roughness was shown in in [4], experimentally and numerically, to increase the flow separation on the suction side of the stator. In [5], a computational study showed that an increase in surface roughness reduced the overall performance of a compressor stage in a design point and that a hub corner separation was affected.

Clearly, an increase in surface roughness can have a large effect on the performance of a compressor stage. The present study aims to increase the understanding of how surface roughness on a level representative of a long time of in-service use affects the design of a compressor stage. The approach is to first optimize a compressor stage considering hydraulically smooth blade surfaces and subsequently increase the surface roughness of a number of optimal blade designs. The robustness of the designs obtained from this first approach in terms of sensitivity to an increased level of surface roughness will be evaluated in a comparison to a second optimization. The second optimization considers a high level of surface roughness from the outset with the same constraints and design space as the first optimization. An optimization process is used to assess the impact of surface roughness since this is a tool commonly use when designing a new compressor stage. Blade designs which meet criteria in a specified design point are found by the optimization process and can be compared in terms of performance. From an industry perspective a study of this characteristic can be of interest to evaluate when the impact of surface roughness needs to be considered in the design phase.

REFERENCE COMPRESSOR STAGE

The reference compressor stage used in the present study is a transonic compressor stage, previously analyzed in [6].

Speedlines generated from CFD calculations of the stage with hydraulically smooth geometries at two rotational speeds, 100% and 58% of the design speed, are shown in Fig. 1. The design point is shown as the intersection of the speedline at design speed and the operating line, where the operating line represents a constant throttle valve setting. Geometrical and performance data for the reference stage at design and part speed are given in Table 1.

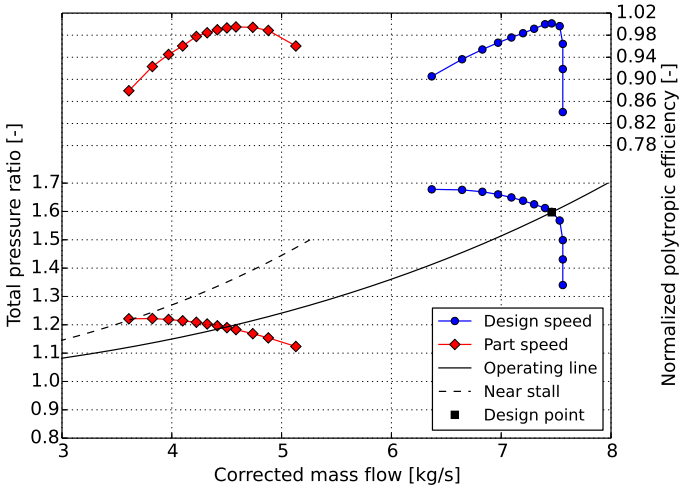

FIGURE 1. COMPRESSOR MAP OF THE REFERENCE STAGE

NUMERICAL METHOD

The CFD calculations are done in the in-house code Volsol++ developed jointly by Chalmers University of Technology and GKN Aerospace. Volsol++ is a density-based, finite-volume solver using a three-stage Runge-Kutta time marching method. The turbulence model used is the realizable k-ε model with the Kato-Launder limiter.

Evaluating one design at part speed or design speed requires approximately $1^1/_2$ hours of computational time. Ten designs are run in parallel on a cluster where 16 cores are used for each simulation. The total computational time sums up to approximately two days for an optimization.

Boundary Conditions

A single rotor and stator blade passage with periodic boundary conditions is used for all simulations. The inlet boundary condition is specified in terms of total pressure, total temperature, turbulence kinetic energy, turbulence dissipation and the direction of the velocity vector. A mixing plane [7], where the flow properties are averaged in the circumferential direction, is used at the interface of the rotor and stator domain. Wall functions are used and the walls are treated as adiabatic. Using the k-ε turbulence model with wall functions showed fairly good agreement with experimental results in [8], giving a conservative performance estimate. A non-reflective boundary condition [9] is used at the outlet. Tip clearances have been neglected and the flow is assumed to be fully turbulent.

For the calculations done with surface roughness, a sand-grain roughness, k_s, of 16 μm is applied on the rotor and stator blades. A sand-grain roughness of 16 μm corresponds to an R_a of approximately 2.6 using the conversion factor given in [10]. At this point, it is appropriate to acknowledge the limitations of converting a sand-grain roughness to R_a and vice versa, as is discussed in [11], and more recently in [12].

TABLE 1. SPECIFICATIONS AND PERFORMANCE DATA FOR THE REFERENCE STAGE.

Rotor aspect ratio	1.4
Rotor hub-tip-ratio	0.8
Rotor solidity	1.2
Design rotational speed	22 456 rpm

Design point

Corrected mass flow	7.48 [kg/s]
Total pressure ratio	1.6
$M_{rotor\ tip,rel}$	1.1
$Re_{chord,rotor}$	1.0×10^6

Part speed

$M_{rotor\ tip,rel}$	0.70
$Re_{chord,rotor}$	4.5×10^5

Wall Roughness Model

Wall roughness is modeled as in the wall roughness model implemented in ANSYS Fluent [13]. The velocity profile, as determined by the law of the wall shown in Eq. 1, is shifted by a value ΔB ($\Delta B = 0$ in the standard law of the wall formulation). Applying a shift of the wall function to model surface roughness was shown in [4] to produce results which compare reasonably well with experimental measurements.

$$u^+ = \frac{1}{\kappa}\ln(y^+) + B - \Delta B \tag{1}$$

The value of ΔB depends on the value of the equivalent sand-grain roughness Reynolds number, k_s^+, defined in Eq. 2.

$$k_s^+ = \frac{u_\tau k_s}{\upsilon} \tag{2}$$

In the Fluent wall roughness model, k_s^+ values between 2.25 and 90 is denoted as the transitional regime. For values above 90 it is considered to be in the fully rough regime. A different function is used to calculate the shift (ΔB) in each region. For values of k_s^+ below 2.25 the wall is considered hydraulically smooth and no shift of the velocity profile is applied. While it is stated in [14] that k_s^+ below 5 is generally considered hydraulically smooth, the model implemented in ANSYS Fluent give consideration to a region of this kind. A different model, which applies a shift of the velocity profile for any $k_s^+ > 0$, is implemented in ANSYS CFX [15].

The wall roughness model in ANSYS Fluent includes a roughness constant, denoted as C_s, which is used to model different roughness characteristics. C_s = 0.5 was used in the present study which corresponds to a uniform sand-grain roughness.

The average k_s^+ on the rotor and stator in the present study at design speed is 25 and 20, respectively. At the part speed condition, the average value is 12 for the rotor blade and 9 for the stator blade.

OPTIMIZATION APPROACH

The design variables used for the rotor and stator blades are the leading and trailing edge blade angles and the blade stagger angle at three spanwise positions (10%, 50% and 95%), resulting in a total of 18 design variables. These variables are allowed to vary approximately $\pm$ 3 degrees around the reference stage.

A transonic compressor stage is optimized using a genetic algorithm [16] in modeFrontier^{TM} to meet design requirements at a specified design point. An initial design set of 190 designs is first generated by latin hypercube sampling. A radial basis function is then generated based on results from CFD calculations of the initial design set. Ten designs are chosen from a converged Pareto front obtained from the optimization made on the response surface. These ten designs are evaluated using CFD calculations and are subsequently used to update the response surface. This process is repeated until the response surface is considered converged. A total of 250 designs were evaluated for each optimization in the present study. The optimization approach used in the present study is described in more detail in [17], where it was shown to be effective in finding compressor blade designs with high performance.

Two design objectives are used to rank the performance of the stages: polytropic efficiency at the design point and part speed stability. The polytropic efficiency at the design point is an appropriate objective since this is the operating condition the compressor stage is designed to operate at most of the time. Part speed stability is used as the second objective to facilitate stable operation as the engine is throttled. Stability is evaluated in terms of the maximum achievable weighted average static pressure recovery in the rotor and stator passage. The weighted average static pressure recovery is defined as shown in Eq. 3, where subscript 0 denotes stagnation condition. Subscripts 1, 2 and 3 denote positions defined in Fig. 2. The formulation is reproduced from [18], without the correction parameter for the minimum dynamic pressure entering the blade row.

$$C_{p,rs} = \frac{(\overline{P}_3 - \overline{P}_2) + (\overline{P}_2 - \overline{P}_1)}{(\overline{P}_{0_2} - \overline{P}_2) + (\overline{P}_{01,rel} - \overline{P}_1)} \tag{3}$$

The optimized designs must be able to reach the design point at the design rotational speed in terms of total pressure ratio and mass flow.

Two optimization approaches are considered in the present study. The first approach is to optimize the performance of a compressor stage with hydraulically smooth blade surfaces. The second is an optimization considering rough blade surfaces, with a level of surface roughness representative of a long time of in-service use.

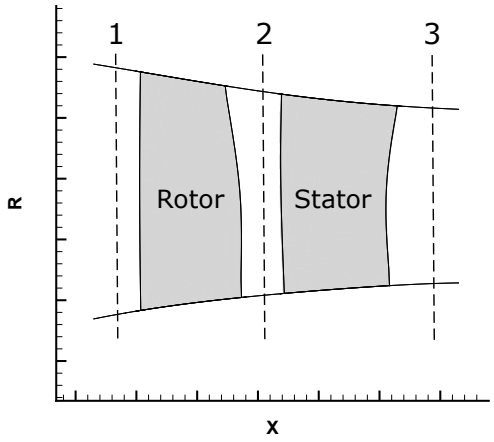

FIGURE 2. THE REFERENCE STAGE WITH NUMBERED LOCATIONS

COMPUTATIONAL GRIDS

The computational grid is made up of hexahedral elements. The boundary layer around the blades is resolved using an O-grid, while the blade passages are constructed using H-type blocks. An example of the computational grid is shown in Fig. 3. The average y+ value of the first node away from the no-slip walls varies in the range of 30 – 60 depending on the operating condition, a region appropriate for use of wall functions.

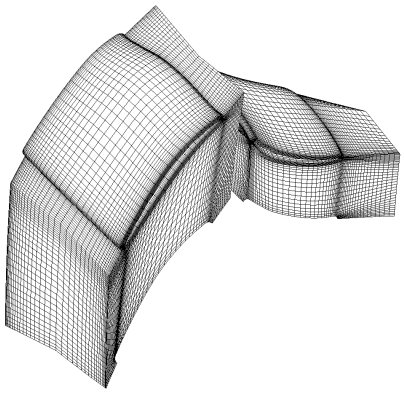

FIGURE 3. COMPUTATIONAL GRID. MEDIUM REFINEMENT. ROTOR (LEFT) AND STATOR (RIGHT).

TABLE 2. NUMBER OF GRID CELLS IN THE ROTOR AND STATOR DOMAINS

Mesh	Rotor cells	Stator cells
Very coarse	25k	32k
Coarse	50k	64k
Medium	100k	100k
Fine	200k	150k

Mesh Study

A mesh sensitivity study is done for the reference stage at design and part speed. Table 2 shows the number of cells used in rotor and stator domains for the different computational grids included in the study. Results of the mesh study are presented in Fig. 4. Mesh independence is evaluated by the performance parameters at the design point (dp) and by the mass flow and static pressure recovery at the intersection of the operating line and the speed line at part speed (ps). The difference shown for the mesh sizes is given in relation to the corresponding performance parameter evaluated for the fine mesh.

It is concluded that mesh independence is achieved for the mesh denoted as *Medium*. The maximum difference in the evaluated performance parameters between the medium and fine mesh is below 0.08%.

RESULTS

Smooth Blade Surfaces

The first approach is an optimization of the reference stage with the blade surfaces assumed to be hydraulically smooth, using the standard wall function to resolve the boundary layers. The Pareto front obtained from the optimization is shown in Fig. 5. The Pareto front shows that an overall increase in stability can be achieved and that a potential increase in polytropic efficiency of 0.7% is possible given the allowed variable range in the optimization. The performance of three designs in the Pareto front, the design with highest efficiency ($\eta_{max,smooth}$), highest stability ($S_{max,smooth}$) and a balanced design ($Balanced_{smooth}$), are listed in Table 3. Note that the performance parameters in Table 3 and Fig. 5 have been normalized with the performance of the reference stage.

For the reference stage, stall is initiated by a separation at the stator hub at both part speed and design speed. Streamlines are projected onto the stator blade surface and Mach numbers are shown for a constant axial position downstream of the stator trailing edge at part speed in Fig. 6 for operating points along the near stall operating line shown in Fig. 1. Low momentum flow from a hub corner separation in the stator is visible for the reference stage in Fig. 6(a). Evidence of a separation is also visible for $\eta_{max,smooth}$ in Fig. 6(b) although to a smaller extent. No evidence of the separation is seen in Fig 6(c) and Fig. 6(d). Further studies, not presented here, showed that a stator hub corner separation was eventually the cause for stall in all four designs at part speed.

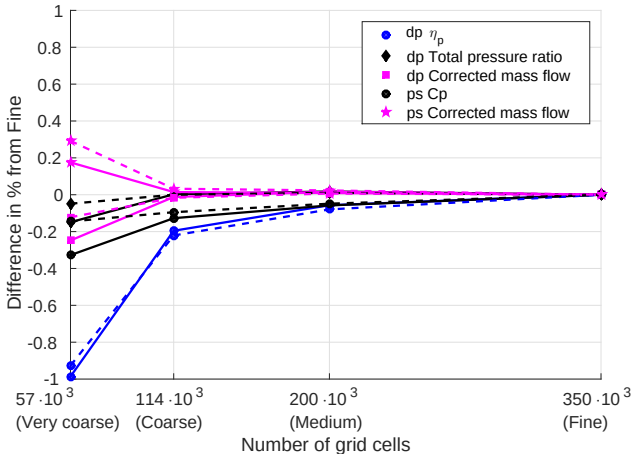

FIGURE 4. MESH STUDY. SOLID LINES = SMOOTH BLADE SURFACES. DASHED LINES = ROUGH BLADE SURFACES.

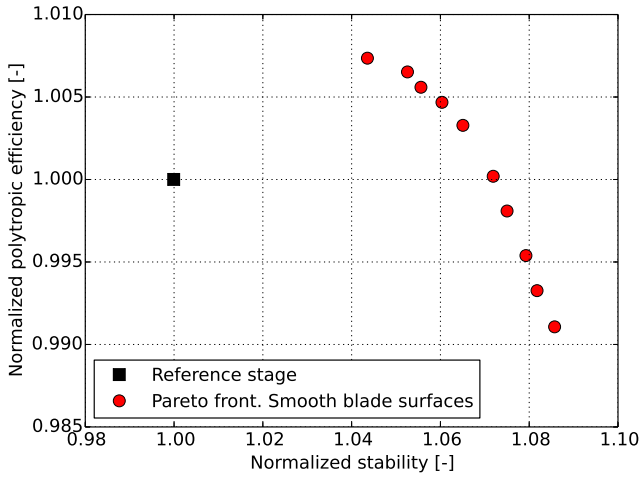

FIGURE 5. PARETO FRONT FROM OPTIMIZATION USING SMOOTH BLADE SURFACES.

Rough Blade Surfaces

Results from an optimization considering rough blade surfaces are presented in this section. The Pareto front for the second optimization approach considering rough blade surfaces is shown in Fig. 7. The performance of three designs, the design with the highest efficiency ($\eta_{max,rough}$), the highest stability ($S_{max,rough}$) and a balanced design ($Balanced_{rough}$), are listed in Table 4.

TABLE 3. PERFORMANCE FOR STAGES OBTAINED FROM OPTIMIZATION USING SMOOTH BLADE SURFACES.

Stage	Normalized η_p [-]	Normalized stability [-]
Reference stage	1.000	1.000
$\eta_{p,max,smooth}$	1.007	1.044
$S_{max,smooth}$	0.991	1.086
$Balanced_{smooth}$	1.003	1.065

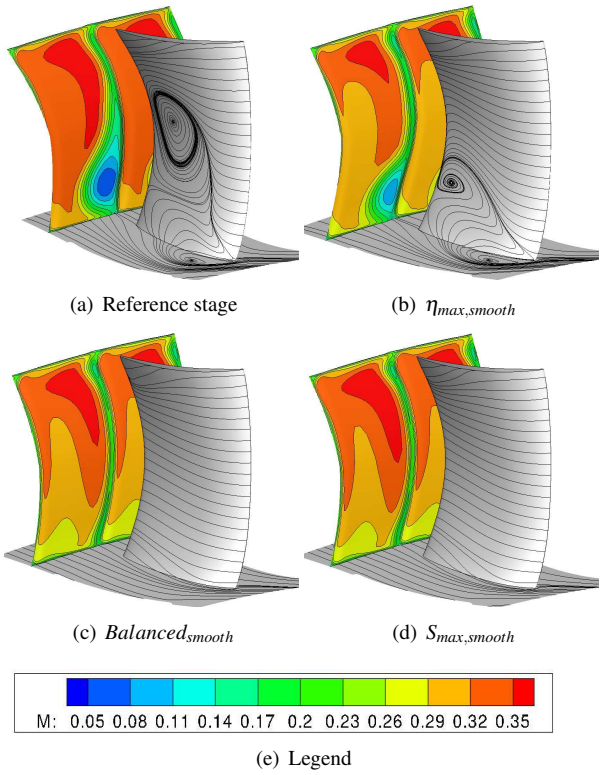

(a) Reference stage (b) $\eta_{max,smooth}$ (c) $Balanced_{smooth}$ (d) $S_{max,smooth}$ (e) Legend

FIGURE 6. STREAMLINES PROJECTED ON THE STATOR BLADE AND MACH NUMBERS ON A PLANE DOWNSTREAM THE BLADE NEAR STALL AT PART SPEED.

Performance Comparison

The design with the highest polytropic efficiency using rough blade surfaces has a 3.5% lower efficiency as compared to the highest efficiency design using smooth blade surfaces. Comparing the stability measure, the design with the highest stability using rough blade surfaces is 3.3% lower than the highest stability design using smooth blade surfaces. The difference in the stability measure is believed to be due to the approach of using the static pressure increase to evaluate stability. Increasing the surface roughness on the blades increases the boundary layer thickness and reduces the amount of diffusion that is possible from the same variations in the design variables.

When the surface roughness is increased on the blade surfaces, the speedline is shifted as losses increase and the effective passage area decreases due to thicker boundary layers. The decrease in polytropic efficiency, mass flow and total pressure ratio for the reference stage that results from increasing the level of surface roughness on the blade surfaces is shown in Fig. 8.

TABLE 4. PERFORMANCE FOR STAGES OBTAINED FROM OPTIMIZATION USING ROUGH BLADE SURFACES.

Stage	Normalized η_p [-]	Normalized stability [-]
$\eta_{p,max,rough}$	0.972	1.031
$S_{max,rough}$	0.966	1.053
$Balanced_{rough}$	0.970	1.044

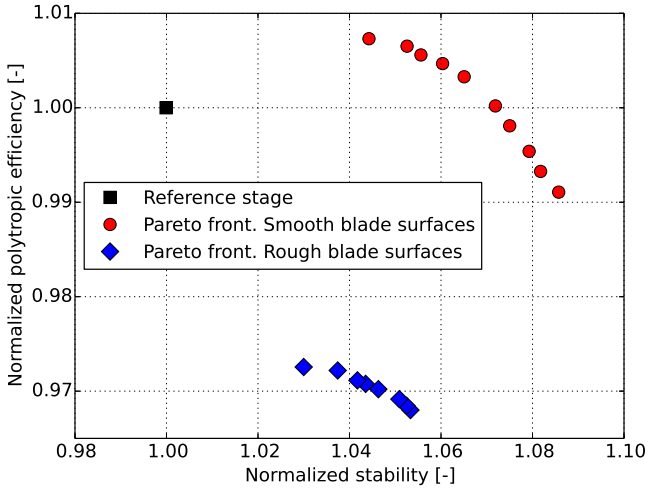

FIGURE 7. PARETO FRONT FROM OPTIMIZATIONS USING SMOOTH AND ROUGH BLADE SURFACES.

The observed shift of the speedline has been reported in previous studies, *e.g.* in [19]. Degrading the blade surfaces is shown to have a larger impact on performance at design speed than at part speed, as was also noted in [2], and it is clear that the design point can no longer be reached at the design rotational speed. The larger difference in the total pressure ratio at design speed compared to part speed was discussed in [2] to be related to a change in the rotor shock system, which plays an important role in increasing the pressure rise at design speed.

The impact of surface roughness on the boundary layer profile also increase for higher free stream velocities as the k_s^+ increase. The stall margin appears to be relatively unaffected for the reference stage (see Fig. 8) by the increase in surface roughness, which is in agreement with previous studies [2, 11] where the stall line was shown to be relatively uneffected by a higher surface roughness.

If the design point cannot be reached at the design rotational speed due to a performance reduction, it could still be possible to reach it by increasing the engine fuel flow. Increasing the fuel burn in the combustion chamber would increase the work that can be extracted from the flow in the turbines, increasing the rotational speed of the shafts (and the connected compressors).

For comparison reasons the geometries listed in Table 3 are degraded by adding surface roughness of the same level as the blades optimized with surface roughness. Surface roughness is considered in the CFD calculations for these designs using the same approach (modified wall function) as for the optimization using rough blade surfaces. The rotational speeds of the degraded compressor stages are increased to approximately 102% of the design speed to reach the design point in terms of mass flow and total pressure ratio. It is important to acknowledge that increasing the rotational speed results in a higher power input to the compressor. Two designs with the same efficiency at different rotational speeds thus require different power inputs. Regardless of the initial design, the rotational speed would have to be increased to reach the design point as the surface roughness of the compressor blades increase. The performance of the degraded compressor stages at the design point is listed in Table 5, where the performance parameters are normalized with the performance of the reference stage with smooth blade surfaces. The performance of the degraded stages is shown in the Pareto front in Fig. 9.

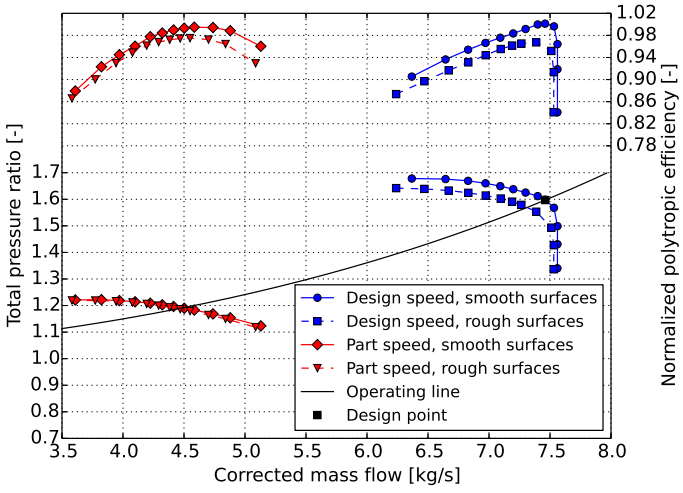

FIGURE 8. COMPRESSOR MAP OF THE REFERENCE STAGE WITH SMOOTH AND ROUGH BLADE SURFACES.

The polytropic efficiency is shown to decrease by approximately 3.5% for the three degraded designs. The geometry of $\eta_{max,smooth}$, which had the highest efficiency along the Pareto front for the smooth designs, is, once degraded, among the highest efficiency points in the Pareto front from the optimization using rough blade surfaces. Similarly, the geometry with the highest stability measure is shown to be one of the top ranked designs in terms of stability when degraded. In fact, the degraded $S_{max,smooth}$ geometry has a higher stability than the other designs with a high surface roughness. The $S_{max,smooth}$ geometry was not found by the optimization using rough blade surfaces since it does not meet the requirement of being able to reach the design point at 100% of the design rotational speed, a criterion enforced on all new designs.

These results indicate that the geometries that perform well with respect to a design objective with smooth blade surfaces still perform well when the surface has been degraded.

Flow Field and Pressure Distribution

The effect of surface roughness on the flow and geometry is investigated further. The stagger angle distribution for designs $\eta_{max,smooth}$ and $\eta_{max,rough}$ is shown in Fig. 10. An overall lower stagger angle can be observed for the rotor blades optimized for a higher level of surface roughness. This decrease compensates for the higher blockage induced by thicker boundary layers. The

TABLE 5. PERFORMANCE OF THE DEGRADED STAGES AT 102% OF DESIGN ROTATIONAL SPEED.

Stage	Normalized η_p [-]	Normalized stability [-]
Reference stage (degraded)	0.962	0.977
$\eta_{p,max,smooth}$ (degraded)	0.971	1.026
$S_{max,smooth}$ (degraded)	0.956	1.059
$Balanced_{smooth}$ (degraded)	0.968	1.044

decrease in stagger makes it possible to reach the design point in terms of mass flow at the design rotational speed. The stagger angle is observed to be approximately the same at the shroud. The leading and trailing edge blade angles (not shown here) are different for the two designs to match the incoming flow, and to facilitate sufficient turning of the flow to reach the design point.

Relative Mach number distributions along the operating line at mid span for $\eta_{max,smooth}$ and the degraded $\eta_{max,smooth}$ stage at design speed are shown in Fig. 11(a) and Fig. 11(b), respectively. The Mach number distribution for the two cases is similar, but it can be noted that a larger region of low momentum flow is visible near the trailing edge of the suction surfaces for the stage with degraded blade surfaces, which is a consequence of the increased surface roughness. It is also shown that the position of the shock on the rotor suction surface is slightly more downstream for the stage with smooth blade surfaces, supporting the discussion in [2] that the surface roughness has an effect on the rotor shock system, which affects the pressure rise more at design speed than at part speed.

Streamlines projected onto the rotor blade suction surface

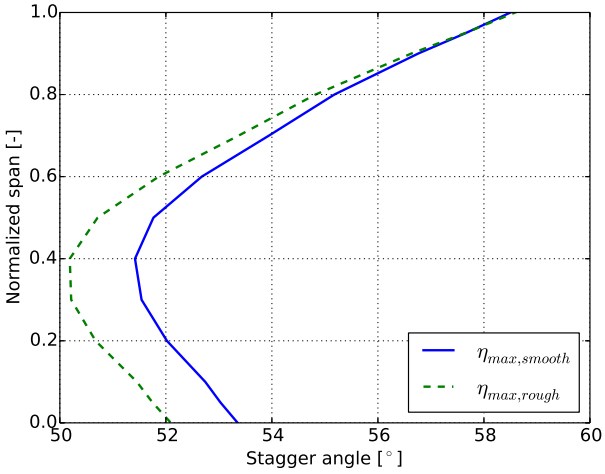

FIGURE 10. ROTOR STAGGER ANGLE DISTRIBUTION.

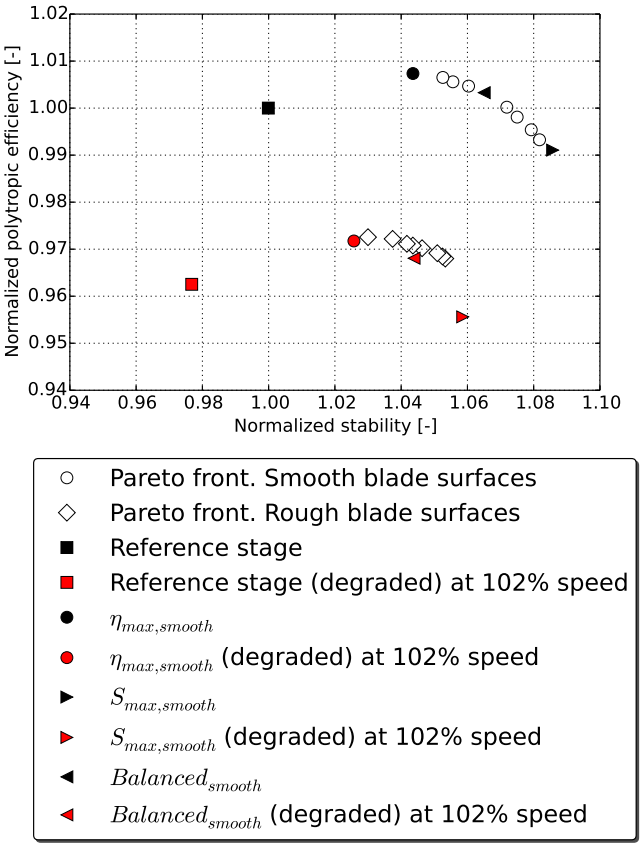

FIGURE 9. PARETO FRONTS INCLUDING PERFORMANCE FOR DEGRADED STAGES.

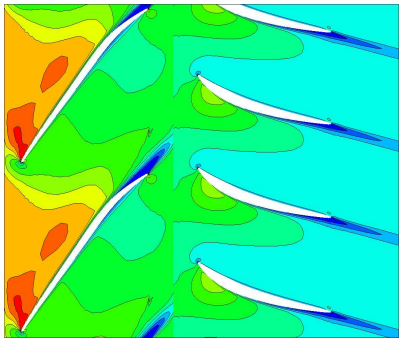

(a) $\eta_{max,smooth}$

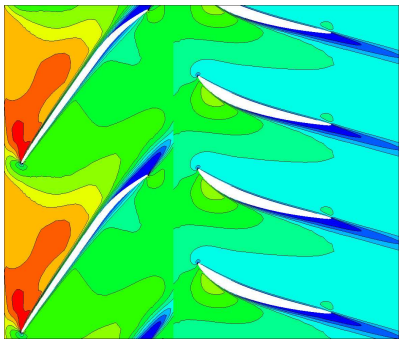

(b) $\eta_{max,smooth}$ (degraded) at design speed

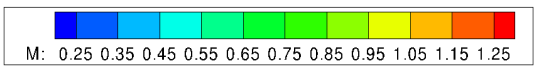

(c) Legend

FIGURE 11. RELATIVE MACH NUMBERS AT MID SPAN.

for $\eta_{max,smooth}$ and the degraded $\eta_{max,smooth}$ stage for operating points that intersect the operating line at design rotational speed are shown in Fig. 12(a) and Fig. 12(b), respectively. Furthermore, contours of constant relative total pressure are plotted at a plane of constant axial position downstream of the rotor. The total pressure contours visualize the thicker wake of the rotor blade with higher surface roughness in Fig. 12(b) compared to the wake of the blade with smooth surfaces in Fig. 12(a). The projected streamlines show that the flow is similar over the suction surface for the two blades, both with a separation near the trailing edge. The general flow topology appears unaffected by the increase in surface roughness.

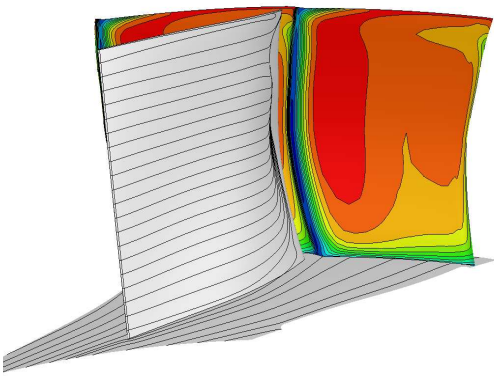

(a) $\eta_{max,smooth}$

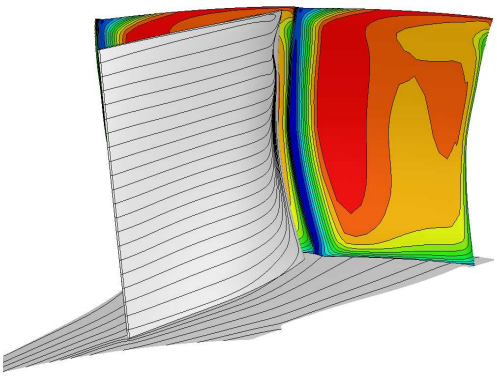

(b) $\eta_{max,smooth}$ (degraded) at design speed

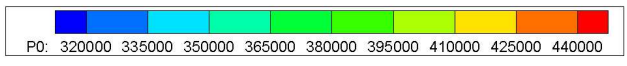

(c) Legend

FIGURE 12. STREAMLINES PROJECTED ON THE ROTOR SUCTION SIDE AND RELATIVE TOTAL PRESSURE CONTOUR DOWNSTREAM OF THE ROTOR.

SUMMARY AND CONCLUSIONS

A transonic compressor stage was optimized using two different approaches. The first approach considered smooth compressor blades while the second approach considered a higher level of surface roughness. It was shown that compressor blades obtained from the first approach still perform well when degraded, and was ranked among the highest performing stages of the Pareto front obtained from the second approach.

An increased surface roughness in itself was shown to have a large effect on performance. However, results in the present study show that it is of relatively low importance to include surface roughness in terms of its impact on the design variables for a compressor blade. This was shown for the chosen design variables and the allowed design space.

Matching of the compressor is affected by a number of uncertainties, where surface roughness variations during the life time of the compressor contribute. Therefore, it could still be of interest to account for the surface roughness in the design phase to ensure matching of the compressor.

ACKNOWLEDGMENT

This work was funded by the Swedish National Aviation Engineering Research Programme, NFFP. The authors would like to acknowledge the financial support of VINNOVA, the Swedish Defense Material Administration (FMV) and GKN Aerospace. The authors would also like to thank the National Supercomputer Center, Linköping, Sweden, and Chalmers Centre for Computational Science and Engineering, Gothenburg, Sweden, for the computational resources required for this work.

REFERENCES

[1] Nikuradse, J., 1950. "Laws of Flow in Rough Pipes, NACA Technical Memorandum 1292".

[2] Suder, K. L., Chima, R. V., Strazisar, A. J., and Roberts, W., 1995. "The Effect of Adding Roughness and Thickness to a Transonic Axial Compressor Rotor". *Journal of Turbomachinery,* ***117***(4), pp. 455–463.

[3] Chul Back, S., Hubson, G. V., Jin Song, S., and Millsaps, K. T., 2012. "Effects of Reynolds Number and Surface Roughness Magnitude and Location on Compressor Cascade Performance". *Journal of Turbomachinery,* ***134***(5), pp. 051013–1–051013–6.

[4] Gbadebo, S. A., Hynes, T. P., and Cumpsty, N. A., 2004. "Influence of Surface Roughness on Three-Dimensional Separation in Axial Compressors". *Journal of Turbomachinery,* ***126***(4), pp. 491–505.

[5] Chinnaswamy, S. "The Impact of Surface Roughness on Transonic Compressor Performance". Master's thesis, Chalmers University of Technology.

[6] Lejon, M., Andersson, N., Martensson, H., and Ellbrant, L., 2015. "CFD Optimization of a Transonic Compressor Stage with a Large Tip Gap". In Proceedings of ISABE 2015, no. ISABE-2015-20038.
[7] Stridh, M., 2006. "Modeling Unsteady Flow Effects in 3D Throughflow Calculations". PhD thesis, Chalmers University of Technology.
[8] Lejon, M., Andersson, N., Eriksson, L.-E., and Ellbrant, L., 2015. "Simulation of Tip-clearane Effects in a Transonic Compressor". In Proceedings of ASME Turbo Expo 2015, no. GT2015-43033.
[9] Engquist, B., and Majda, A., 1977. "Absorbing Boundary Conditions for the Numerical Simulation of Waves". *Mathematics of Computation,* ***31***(139), pp. 629–651.
[10] Koch, C., and Smith, Jr., L. H., 1976. "Loss Sources and Magnitudes in Axial-Flow Compressors". *Journal of Engineering for Power,* ***98***(3), pp. 411–424.
[11] Schaffler, A., 1980. "Experimental and Analytical Investigation of the Effects of Reynolds Number and Blade Surface Roughness on Multistage Axial Flow Compressors". *Journal of Engineering for Power,* ***102***(1), pp. 5–12.
[12] Goodhand, M. N., Walton, K., Blunt, L., Lung, H. W., Miller, R. J., and Marsden, R., 2015. "The Limitations of Using R_A to Describe Surface Roughness". In Proceedings of ASME Turbo Expo 2015, no. GT2015-43329.
[13] ANSYS Fluent User's Guide Version 15.0, ANSYS Inc. 2014.
[14] Schlichting, H., and Gersten, K. *Boundary Layer Theory*. Springer-Verlag Berlin and Heidelberg GmbH & Co. K.
[15] ANSYS CFX-Solver Theory Guide Version 15.0, ANSYS Inc. 2014.
[16] Deb, K., Pratap, A., Agarwal, S., and Meyarivan, T., 2000. A Fast and Elitist Multi-Objective Genetic Algorithm: NSGA-II. Tech. rep., Indian Institute of Technology Kanpur. KanGAL Report No. 200001.
[17] Ellbrant, L., Eriksson, L.-E., and Martensson, H., 2013. "Balancing Efficiency and Stability in the Design of Transonic Compressor Stages". In Proceedings of ASME Turbo Expo 2013.
[18] Smith, Jr., L. H., 2001. Compressor Aero Design at General Electric before CFD. ISABE-2001-1002.
[19] Bammert, K., and Woelk, G. U., 1980. "The Influence of the Blading Surface Roughness on the Aerodynamic Behavior and Characteristic of an Axial Compressor". *Journal of Engineering for Power,* ***102***(2), pp. 283–287.